International Journal of Engineering & Technology, 7 (3.32) (2018) 153-156

SPC

International Journal of Engineering & Technology

Website: www.sciencepubco.com/index.php/IJET

Research paper

Facile synthesis of g-CN/ATO hybrid nanocomposite and its application for the photodegradation of organic compounds

Devi Prashad Ojha[a], JunHee Song[a *], Han Joo Kim[a,b*]

[a]Department of Convergence Technology Engineering, Chonbuk National University, Jeonju 561-756, Republic of Korea
[b]Eco-friendly Machine Parts Design Center, Chonbuk National University, Jeonju 561-756, Republic of Korea
**Corresponding author E-mail:sjhee@jbnu.ac.kr*

Abstract

Photodegradation of organic pollutants using nanoparticles with suitable band gap is one of the most studied technologies in last few decades. About 6 nm antimony-doped tin oxide (ATO) nanoparticles, as the photocatalyst for organic degradation, is prepared by the calcination of the stoichiometric mixture of precursor hydroxides of Sn^{4+} and Sn^{3+}. ATO was combined with thermally synthesized g-C_3N_4 and the resulting Z-scheme g-CN/ATO nanocomposite was utilized for the decomposition of salicylic acid (SA) in aqueous solution. All the samples were analyzed by scanning electron microscopy (SEM), transmission electron microscopy (TEM), X-ray diffraction (XRD), energy dispersive spectroscopy (EDS), Fourier transform infrared spectroscopy (FTIR) and the progress of the photocatalytic degradation reaction was measured by using UV-Visible spectroscopy. The rate constant measurements showed that the rate of degradation of SA is enhanced with hybrid nanocomposite.

Keywords: *Antimony-doped tin oxide (ATO), graphitic carbon nitride (g-CN), Salicylic acid (SA), and photocatalyst.*

1. Introduction

Heterogeneous photocatalysis has been regarded as the sustainable renewable technology to solve the global energy and environmental crisis, in which semiconductor materials generate reactive electron-hole pair by band gap excitation in presence of sunlight [1]. TiO_2 is considered most promising photocatalyst due to its low cost, high stability and non-toxicity as well as suitably placed band position and excellent surface properties. However, practical application of TiO_2 is hindered due to its wide band gap (Eg = 3.2 eV) which can only absorb UV light ($\lambda < 380$ nm) which is merely a 4% of the whole sunlight [2-5]. Thus quest of alternative photocatalysts that can utilize the major portion of the sunlight i.e. visible light is another major strategy in the photocatalysis. Antimony doped tin oxide ($Sb.SnO_2$: ATO) is one such semiconductor with excellent charge mobility and narrow band gap (E_g = 2.65 eV) that can absorb major portion of sunlight [6, 7]. However, firstly the band position of ATO is not appropriately placed with conduction band (CB, +0.95 V) and valence band (VB, +3.6 V); it cannot generate the reactive species in aqueous medium. Secondly, the recombination of electron-hole is faster than the electron transport [8].

Coupling of two semiconductors with matching band position can decrease the recombination rate due to the charge transfer and thus the photogenerated electron-hole pair becomes more available for higher catalytic efficiency [9, 10]. A notable strategy to overcome this limitation was applied by combining it with TiO_2 for the decomposition of Methylene Blue in a visible-light photocatalytic mechanism [11]. Next, graphitic carbon nitride (g-C_3N_4) could be a potential material for yet another strategy. g-C_3N_4 has sufficiently negative conduction band position to utilize the photogenerated electron and its exfoliated 2D flat-structure provides more reactive sites that reduces e-h recombination rate [12]. Thus a new z-scheme type ATO/g-C_3N_4 system is designed. The photocatalytic decomposition of a model organic compound salicylic acid (SA) was studied and the origin of the enhanced photoactivity was suggested in a mechanism.

2. Material and methods

2.1. Materials

All the reagents, melamine, tin chloride ($SnCl_4.5H_2O$), sodium bicarbonate (NH_4HCO_3), acetic acid (CH_3COOH), antimony chloride ($SbCl_3$), ethanol, salicylic acid (SA) and NH_4OH were purchased from Sigma-Aldrich and used directly for experiments without any further purification.

2.2. Synthesis of g-C_3N_4 nanosheet

Melamine was thermally polymerized at 550 °C for 3 hours in a muffle furnace resulting yellowish graphitic carbon nitride (g-C_3N_4) [13]. g-C_3N_4 powder was crushed into fine powder and again heated at 550 °C for 3 hr to complete the polymerization of the remaining melamine. Next, the bulk g-C_3N_4 powder was stirred overnight with oxalic acid (1.0 M). Thus exfoliated g-C_3N_4 nanosheet was separated from the suspension by filtration, freeze-dried and heated at 300 ^oC to remove the residual oxalic acid.

2.3. Synthesis of ATO nanoparticles and ATO/gCN nanocomposite

In the synthesis of ATO nanoparticles as reported in [14], 50 ml of ethanol was vigorously stirred with 3.25g of $SnCl_4 \cdot 5H_2O$, 5 mol % $SbCl_3$, 5.5g NH_4HCO_3 and 1.75 g CH_3COOH in a 100 ml beaker for 4 hours. The pH of the solution was adjusted at 7 by adding ammonia solution. The white suspension of the $Sn(OH)_4$ and $Sb(OH)_3$ was centrifuged and washed 3 times with distilled water and calcined at 550 °C for 8 h. The bluish grey powder confirmed the formation of ATO nanopowder.
For the synthesis of ATO/gCN nanocomposite, ATO NP and g-CN were separately sonicated in ethanol: water (1:1) solution for 30 min and mixed together before a hydrothermal treatment at 180 °C for 4 hour. The resulting composite with 1%, 5% and 10% by weight of g-CN was washed several times and dried.

2.4. Characterization

The crystal phase of the prepared samples was identified by X-ray powder diffraction (Rigaku Multiflex diffractometer). Likewise the surface morphology of all samples was analyzed by a field-emission scanning electron microscope (FE-SEM, S-7400, Hitachi, Japan). Furthermore, the morphology and crystal phase were also analyzed using high-resolution transmission electron microscope (HRTEM, JEM-2010F-JEOL Japan).

2.5. Photocatalytic measurement

The photoactivity of the samples was studied in terms of the photodegradation of SA with visible light source [15]. 1 mg/l of the catalyst and 50 ml of the 10 mg/l SA aqueous solution were stirred in a 100 ml photo-reactor for 30 min in dark to attain the adsorption-desorption equilibrium between the catalyst and SA. The solution was irradiated with visible light from A 300 W Xe lamp (DY. Tech., Korea) equipped with a UV and IR cut-off filters (Edmund optics, USA). After certain time interval, 2 ml aliquot of the solution was drawn out with a syringe fitted with a filter and the absorbance was measured in a UV-Visible spectrophotometer. The concentration of the remaining SA corresponding to the the absorbance at 297 nm was calculated from the Beer-Lambert Law. Finally the rate of the photodegradation of the various samples was compared by the following equation:

$$Degradation\ efficiency\ (\%) = 1 - \frac{C}{Co} \times 100\%$$

Here, C_0 is the concentration of SA at 0 min, and C is the concentration of residual SA at a certain time (t). The dark reaction was also performed for the comparison.

3. Results and discussion

3.1. Morphological studies

XRD pattern in Fig. 1a shows the diffraction peaks of SnO_2 with tetragonal rutile structure corresponding to the JCPDS card number 01-072-1147. No impurity peaks related to Sb_2O_3 or Sb_2O_5 and the bluish grey color of the powder indicated successful doping of Sb on the crystal lattice of SnO_2 and indicated the presence of the new energy band of ATO below the conduction band mimima , originated from outer orbitals (5d and 6s) of Sb. Thus the CB minima of SnO_2 is lowered and also band gap of ATO as 2.55 eV [16]. XRD pattern of 10% ATO/g-CN composites revealed no characteristic diffraction g-CN in the nanocomposite likely due to the low g-CN content (Fig. 1b) [17].

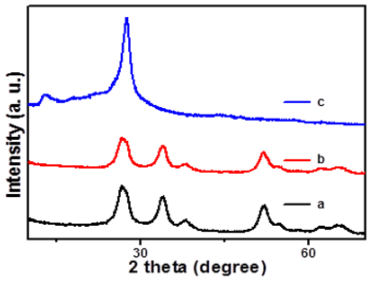

Fig. 1: XRD spectra of (a) ATO nanoparticles, (b) 10%ATO/g-CN nanocomposite and (c) g-CN sheet.

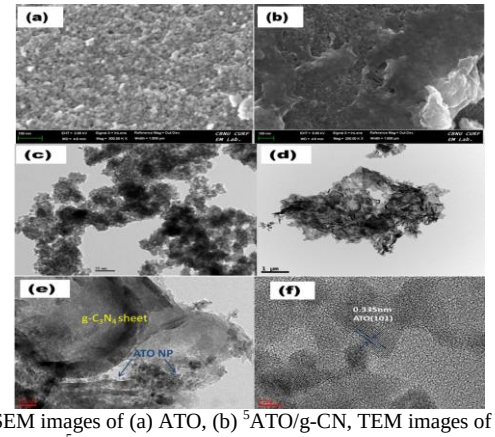

Fig. 2: SEM images of (a) ATO, (b) [5]ATO/g-CN, TEM images of (c) ATO, (d) g-CN, (e) [5]ATO/g-CN nanocomposite and (f) HRTEM image of [5]ATO/g-CN nanocomposite.

The shape size and the crystalline nature of the as-prepared nanoparticle and nanocomposites were investigated in detail by FESEM and TEM/HRTEM (Fig. 2). Fig. 2a and 2b showed FESEM images of monodispersed ATO with high aggregation and ATO/g-CN nanocomposite respectively. The image of ATO/g-CN nanocomposite shows the good attachment of ATO nanoparticles and the g-CN sheet. The intercalation of ATO NPs on g-CN sheet resulted in less agglomeration in the nanocomposite which would significantly increase the surface area and surface characteristics like porosity of the nanocomposite compared to individual components. A TEM image in Fig. 2c shows of clusters of uniform 6 nm ATO nanoparticles. Fig. 2d shows the TEM image of exfoliated g-CN sheet. Fig. 2e shows the TEM image of the [5]ATO/g-CN nanocomposite [18]. HRTEM of [5]ATO/g-CN nanocomposite (Fig. 2f) shows well-developed lattice fringes of ATO nanoparticles which underlines high crystallinity. The d-spacing of 0.335 nm corresponds to the 101 plane of the tetragonal rutile crystal (JCPDS: #01-072-1147).

3.2. Photocatalytic activity

The photodecomposition of SA with different samples was assessed under visible-light irradiation. The concentration of the remnant SA was quantified from the absorption peak at 297 nm in the UV-Visible spectra with respect to different samples. Then, the concentration of solution with several photocatalytic samples was plotted as a function of photoreaction time as displayed in (Fig. 3).

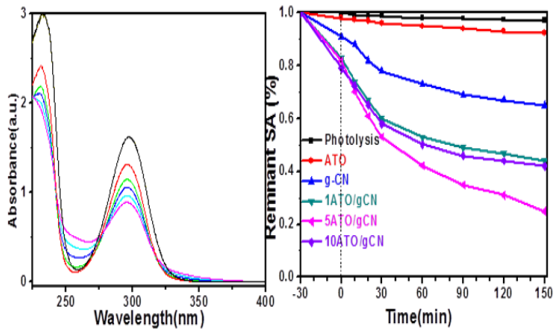

Fig. 3: (a) The Absorption spectra of SA degradation over ^{5}ATO/g-CN, and the Photoactivity of different samples.

ATO/g-CN nanocomposites demonstrated higher photoactivity than the bare ATO or g-CN. Approximately 75% of SA was removed in the 1.5 hr irradiation time, whereas the bare ATO or g-CN could only remove 9% and 38% respectively. The photoactivity of ATO/g-CN nanocomposites is increased by increasing the g-CN content of 1-5 wt % by weight however it is decreased in 10% ATO/g-CN nanocomposite (Fig. 3b). In brief, approximately 48%, 75%, and 54% of the SA is mineralized by 1%, 5% and 10% ATO/g-CN nanocomposites respectively in 1.5 hr photoreaction time.

Based on the above results, the photocatalytic mechanism of ^{5}ATO/g-CN nanocomposite was discussed (Fig. 4). The narrow band gap ATO nanoparticles (2.65eV) and g-CN (2.6eV) can both absorb visible light leading to the formation of e-h pairs. Since the CB minimum of the g-CN (-1.13V) is quite negative compared to that of ATO (+0.95 V), the photogenerated electrons from the CB of g-CN to the CB of ATO cannot jump due to the steep downhill in the energy level, but CB electron of ATO easily jump to the VB of g-CN (+1.47 V). In this way, the recombination rate in both semiconductors is significantly decreased.

This suggests to the well-known Z-scheme photodegradation process in which the holes in the VB of ATO (+2.9V) and the electrons in the CB of g-CN take part in the degradation process. This leads to the reduction of O_2 at the CB of g-C_3N_4 to produce the active species superoxide ($^{\bullet}O_2^-$) and oxidation of water to the hydroxyl ($^{\bullet}$OH) radical [19]. These reactive species subsequently oxidize the adsorbed SA on photocatalyst surface. Additionally holes generated in the ATO VB also oxidize SA to CO_2 and H_2O and other simpler inorganic molecules. Thus hydroxyl ($^{\bullet}$OH), superoxide ($^{\bullet}O_2^-$) and h^+ are the three predominant active species responsible for the enhanced photodegradation of SA as elaborated in the following equations:

Photo-excitation:

Photocatalyst + hv → (e^- + h^+)

Photo-reduction:

$O_2 + e^- \rightarrow {}^{\bullet}O_2^-$,

$^{\bullet}O_2^- + e^- + 2H^+ \rightarrow H_2O_2$,

$H_2O_2 + e^- \rightarrow {}^{\bullet}OH + OH^-$

Photo-oxidation:

$2h^+ + H_2O \rightarrow 2H^+ + {}^{\bullet}OH$

Photo-degradation:

$^{\bullet}O_2^-$, $^{\bullet}$OH, + SA → Degradation products.

On the basis of above experiments the photocatalytic scheme has been designed as shown in fig. 4.

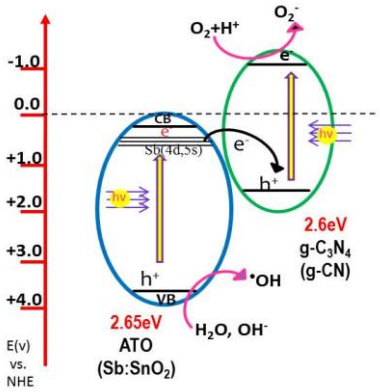

Fig. 4: ATO/g-CN Z-scheme mechanism

4. Conclusion

Thus, monodisperse 6 nm bluish ATO nanoparticles were synthesized and applied with g-C_3N_4 for the photocatalysis. Z-scheme ATO/g-CN nanocomposite showed the higher photoactivity compared to the ATO nanoparticles towards salicylic acid mineralization. The higher photocatalytic activity of ATO/g-CN over g-CN and ATO under visible light irradiation is attributed to the well-aligned band position and increased surface properties. This ultimately accelerated charge-carrier transfer rate, lowered recombination rate and subsequently enhanced photoactivity.

Acknowledgement

Work is supported by a grant from the Korean Ministry of Education, Science, and Technology (MEST) through the National Research Foundation (NRF) (Project No. 2017-R1C1B2011968).

References

[1] W.Z. Tang, Z. Zhang, H. An, M.O. Quintana, D.F. Torres, TiO2/UV Photodegradation of Azo Dyes in Aqueous Solutions, Environmental Technology, 18 (1997) 1-12.

[2] A. Kudo, Y. Miseki, Heterogeneous photocatalyst materials for water splitting, Chemical Society Reviews, 38 (2009) 253-278.

[3] H. Kazuhito, I. Hiroshi, F. Akira, TiO 2 Photocatalysis: A Historical Overview and Future Prospects, Japanese Journal of Applied Physics, 44 (2005) 8269.

[4] P. Pichat, CHAPTER 12 An Overview of the Potential Applications of TiO2 Photocatalysis for Food Packaging, Medical Implants, and Chemical Compound Delivery, in: Photocatalysis: Applications, The Royal Society of Chemistry, 2016, pp. 345-367.

[5] M. Anpo, M. Takeuchi, The design and development of highly reactive titanium oxide photocatalysts operating under visible light irradiation, Journal of Catalysis, 216 (2003) 505-516.

[6] Y. Sun, W.D. Chemelewski, S.P. Berglund, C. Li, H. He, G. Shi, C.B. Mullins, Antimony-Doped Tin Oxide Nanorods as a Transparent Conducting Electrode for Enhancing Photoelectrochemical Oxidation of Water by Hematite, ACS Applied Materials & Interfaces, 6 (2014) 5494-5499.

[7] J. Zhang, L. Gao, Synthesis and characterization of antimony-doped tin oxide (ATO) nanoparticles, Inorganic Chemistry Communications, 7 (2004) 91-93.

[8] D.P. Ojha, H.P. Karki, H.J. Kim, Design of ternary hybrid ATO/g-C3N4/TiO2 nanocomposite for visible-light-driven photocatalysis, Journal of Industrial and Engineering Chemistry, 61 (2018) 87-96.

[9] J. Schneider, M. Matsuoka, M. Takeuchi, J. Zhang, Y. Horiuchi, M. Anpo, D.W. Bahnemann, Understanding TiO2 photocatalysis: mechanisms and materials, Chemical Reviews, 114 (2014) 9919-9986.

[10] L. Yuan, C. Han, M. Pagliaro, Y.-J. Xu, Origin of enhancing the photocatalytic performance of TiO2 for artificial photoreduction of CO2 through a SiO2 coating strategy, The Journal of Physical Chemistry C, 120 (2015) 265-273.
[11] V.J.P. Vilar, C.C. Amorim, G. Li Puma, S. Malato, D.D. Dionysiou, Intensification of photocatalytic processes for niche applications in the area of water, wastewater and air treatment, Chemical Engineering Journal, 310, Part 2 (2017) 329-330.
[12] S. Cao, J. Low, J. Yu, M. Jaroniec, Polymeric Photocatalysts Based on Graphitic Carbon Nitride, Advanced Materials, 27 (2015) 2150-2176.
[13] J. Mao, L. Zhang, H. Wang, Q. Zhang, W. Zhang, P. Li, Facile fabrication of nanosized graphitic carbon nitride sheets with efficient charge separation for mitigation of toxic pollutant, Chemical Engineering Journal, 342 (2018) 30-40.
[14] F. Bai, Y. He, P. He, Y. Tang, Z. Jia, One-step synthesis of monodispersed antimony-doped tin oxide suspension, Materials Letters, 60 (2006) 3126-3129.
[15] D.P. Ojha, M.K. Joshi, H.J. Kim, Photo-Fenton degradation of organic pollutants using a zinc oxide decorated iron oxide/reduced graphene oxide nanocomposite, Ceramics International, 43 (2017) 1290-1297.
[16] M.P.S. Rana, F. Singh, K. Joshi, S. Negi, R.C. Ramola, Influence of electronic excitations on structural, optical and electrical properties of undoped and antimony doped tin oxide thin films, Thin Solid Films, 616 (2016) 34-42.
[17] M.J. Muñoz-Batista, M.N. Gómez-Cerezo, A. Kubacka, D. Tudela, M. Fernández-García, Role of Interface Contact in CeO2–TiO2 Photocatalytic Composite Materials, ACS Catalysis, 4 (2014) 63-72.
[18] Y. Chen, W. Huang, D. He, Y. Situ, H. Huang, Construction of Heterostructured g-C3N4/Ag/TiO2 Microspheres with Enhanced Photocatalysis Performance under Visible-Light Irradiation, ACS applied materials & interfaces, 6 (2014) 14405-14414.
[19] J. Zhang, Y. Nosaka, Mechanism of the OH radical generation in photocatalysis with TiO2 of different crystalline types, The Journal of Physical Chemistry C, 118 (2014) 10824-10832.